Meso Scale Model for Fiber-Reinforced-Concrete: Microplane Based Approach

Smolčić, Željko; Ožbolt, Joško

Meso Scale Model for Fiber-Reinforced-Concrete: Microplane Based Approach

Željko Smolčić [1] **and Joško Ožbolt** [*1,2]

[1] *Faculty of Civil Engineering of University of Rijeka, Radmile Matejčić 3, Rijeka, Croatia*
[2] *Institut für Werkstoffe im Bauwesen, Universität Stuttgart, Pfaffenwaldring 4, Stuttgart, Germany*

Abstract. In the present paper experimental and numerical analysis of hook-ended steel fiber reinforced concrete is carried out. The experimental tests are performed on notched beams loaded in 3-point bending using fiber volume fractions up to 1.5 %. The numerical analysis of fiber reinforced concrete beams is performed at meso scale. The concrete is discretized with 3D solid finite elements and microplane model is used as a constitutive law. The fibers are modelled by randomly generated 1D truss finite elements, which are connected with concrete matrix by discrete bond-slip relationship. It is demonstrated that the presented approach, which is based on the modelling of concrete matrix using microplane model, able to realistically replicate experimental results. In all investigated cases failure is due to the pull-out of fibers. It is shown that with increase of volume content of fibers the effective bond strength and slip capacity of fibers decreases.

1. Introduction

Fiber reinforced concrete is a composite material, to which, in addition to the usual concrete ingredients, small discontinuous fibers of high tensile strength are added during the mixing process. The fibers used in fiber reinforced concrete are classified according to the material they are made of: steel fibers, glass fibers, synthetic fibers and natural fibers (ACI Committee 544 2001). Compared to the same concrete composition without fibers, fiber reinforced concrete has significantly higher fracture energy but also compressive and tensile strengths are higher. However, for some fiber types or for excessively large volume fractions of fibers, compressive or tensile strengths might be reduced. The main advantages of fiber reinforced concrete are visible at the post peak response, when the fibers bridge the cracks and contribute to the resistance and ductility (ACI Committee 544 2001).

Due to its composition concrete is an extremely heterogeneous quasi-brittle material, not simple to model realistically. From the numerical point of view this makes the modelling even more complex. In the numerical modelling macro scale models are mostly used in engineering practice, however, numerically more demanding meso scale models provide better insight into the

---

∗Corresponding author, Ph.D., E-mail: ozbolt@iwb.uni-stuttgart.de

actual concrete behaviour. Numerical studies are essential to improve the properties of the material, such as concrete or fiber reinforced concrete. Having a realistic numerical model, numerical parametric studies together with experiments can serve as important tool to improve material and structural properties. An overview of the models for modelling of fiber reinforced concrete is given in Kunieda *et al*. (2011), according to which the majority of fiber reinforced concrete models are based on: (1) Models formulated in the framework of continuum mechanics using stress-strain (σ-ε) relationship and smeared crack approach (Han *et al*. 2003, Suwada and Fukuyama 2006); (2) Discrete models based on the stress-crack opening law (σ-w, discrete cracks) (Fischer *et al*. 2007, Maalej 2001) and (3) The combination of (1) and (2) (Bolander and Saito 1997).

The numerical analysis of fiber reinforced concrete can be carried out at the macro or meso scale. For the modelling at the macro scale material properties have to be be homogenised and, depending whether the cracking is modelled using smeared or discrete approach, stress-strain softening law or stress-crack opening law is employed. These models are suitable for analysis of structures (e.g. beams, frames, slabs, etc.). As an example for the modelling of the fiber reinforced concrete within the concept of smeared crack approach at the macro scale, where the effect of fibers is implicitly accounted for in the constitutive law, is the recently proposed microplane model M7f (Caner *et al*. 2013). However, when modelling at the meso scale, the fiber reinforced concrete is usually considered as a three - phase material consisting of: cement matrix (concrete), fibers and interface between cement matrix and fibers. Every single fiber has to be modelled separately so that the fiber position and its orientation, as random variables, have to be specified. In such detailed models where the concrete, fibers and its connection (bond) are explicitly discretized (e.g. using finite elements) and characterised by the specific constitutive law, the macroscopic response is the result of the meso scale analysis. These models are useful for detailed parametric studies, however, they are computationally too expensive to be employed in structural analysis. Typical examples of such modelling approach are based on the Lattice models and the Rigid-Body-Spring Model (RBSM) (Kunieda *et al*. 2011, Ogura *et al*. 2013, Bolander and Saito 1997, Jun and Mechtcherine 2010, Bolander and Sukumar 2005, Bolander *et al*. 2008, Kang *et al*. 2014, Schauffert and Cusatis 2012, Schauffert *et al*. 2012).

In the present paper experimental and numerical results of 3-point bending pre-notched beams made of fiber reinforced concrete are presented and discussed. In order to provide better insight into the actual behaviour of fiber reinforced concrete, the numerical analysis is performed at the meso scale. The aim is to investigate whether the meso scale model based on the microplane model for matrix (concrete) is able to replicate the macroscopic response of concrete and to investigate the effective bond-slip relationship between fibers and concrete for different volume content of fibers. In the analysis fiber reinforced concrete is considered as a three-phase composite consisting of concrete, fibers and the interface between them. Concrete is discretized by 3D four nodes constant strain finite elements with the microplane model as a constitutive law (Ožbolt *et al*., 2001). The fibers are modelled as a simple truss finite elements that are randomly distributed over the concrete and represented by the uniaxial stress-strain relationship for steel. The connection between concrete and fibers is modelled with discrete bond-slip relationship. The calibration of the parameters for concrete and for the bond-slip relationship is obtained by fitting experimental results of concrete beams without and with different fiber content. Finally, numerical parametric study is carried out to find out the relationship between volume content of fibers and effective bond-slip relationship. The results indicate that effective bond strength and slip capacity degrade with an increase in volume content of fibers, beyond a threshold value.

2. Experimental investigations

Three-point bending tests are performed on pre-notched fiber reinforced concrete beams. In the experiments the concrete quality is kept constant and only the volume content of steel fibers is varied in the range from 0 to 1.5 %. The experimental results are then used to calibrate numerical model in order to investigate the influence of volume content of fibers on the effective bond-slip constitutive law for fibers.

2.1 Material properties

The compressive strength of concrete is measured according to EN 12390-3 standard (EN 12390-3:2001 2001) on three concrete cubes dimensions 150x150x150 mm. Tensile strength is measured by employing tensile splitting tests according to EN-12390-6 standard (EN 12390-6:2000 2000) on 150x150x150 mm concrete cubes using three specimens. The mean values of compressive and tensile splitting strength are f_c=74.47 MPa and f_{ts}=4.38 MPa, respectively.

In the fiber reinforced concrete the hooked-end steel fibers Dramix RC 65/35 BN are used. The fiber length being $l_f = 35$ mm, the diameter $d_f = 0.55$ mm (Fig. 1) and the aspect ratio $l_f/d_f = 65$. The fiber tensile strength is $f_s = 1.345$ GPa and Young's modulus $E_s = 210$ GPa. To obtain bond-slip relation of a single fiber, three pull-out tests are carried out on 40x40x160 mm concrete prisms (Fig. 2). The steel fibers were embedded in the middle of the concrete prism, with the embedment length equal to one fourth of the fiber length ($l_e = l_f/4 = 35/4 \approx 9$ mm). The axis of the fiber is perpendicular to the surface of the concrete specimen. The pull-out tests are carried out by displacement control, the constant displacement rate being 0.005 mm/s. The experiment is conducted until the fiber is completely pulled out from the specimen (total displacement of 9 mm). The measured pull-out load vs. fiber displacement curves and the corresponding mean value curve are shown in Fig. 3. Note the presence of the post-peak hump, which is characteristic of the actions of the hook-ended of the fiber during pull-out. Note that due to the averaging of test data (n =3) the hump is not clearly seen in the average response curve. The post peak hump is a consequence of fully straightened end of hooked fiber.

2.2 Three-point bending tests on pre-notched beams

The bending tests are carried out on square cross-section beams dimensions bx$h = 150$x150 mm of the total length $L = 550$ mm. The beam is simply supported with the span of $l = 500$ mm (see Fig. 4), according to RILEM recommendations for fiber reinforced concrete structures TC 162-TDF (Vandewalle 2002). The notch at the mid-length of the beam was cut 28 days after casting using the wet sawing method. The beam was turned on its side at 90° against the casting surface and the notch was sawn over the entire width. The notch width is 5 mm and 25 mm in depth (see Fig. 4).

The beam is loaded by displacement control with displacement rate at the mid-span of 0.01 mm/min for plain concrete beams and 0.2 mm/min for the fiber reinforced beams, respectively. For fiber reinforced beams the displacement controlled test is carried out up to the total displacement of approximately 30 mm. During the test the load and displacement at the bottom surface of the beam were continuously measured (see Fig. 5). The tests are performed for four different fiber

volume fractions (V_f = 0%, 0.5%, 1.0% and 1.5%) and for each fiber fraction three specimens are tested, i.e. in total 12 specimens.

Experimentally obtained load-deflection curves for the beams, with different fiber volume fractions (V_f=0%, 0.5%, 1.0% and 1.5%) are plotted in Fig. 6. Each figure shows the load-displacement relationship for all tested specimens as well as the mean value (in black). For plain concrete beams (V_f=0 %) the displacement up to 0.5 mm is shown, while for fiber reinforced concrete (V_f=0.5%, 1.0% and 1.5%) the displacement up to 5.0 mm is plotted. It can be seen that up to the formation of the first crack in concrete the load-displacement curves are almost identical for all beams, and only after the first crack appearance large scatter of measured data can be observed. As expected, with addition of steel fibers the beam response becomes more ductile. It is obvious that with increasing the fiber volume fraction, the resistance and ductility of the beams increase. In all cases the failure is due to the mode-I fracture with formation of single discrete crack.

3. Meso scale modelling approach

In the numerical 3D finite element analysis at the meso scale, fiber reinforced concrete is considered as a three-phase composite consisting of concrete, fibers and the discrete interface between them. Concrete is discretized by 3D finite elements with the microplane model as a constitutive law. The fibers are modelled as simple 1D truss finite elements that are randomly distributed over the concrete and the uniaxial stress-strain relationship for steel is used as a constitutive law. The connection between concrete and fibers is simulated with discrete bond-slip relationship.

3.1 Concrete

The numerical analysis is carried out using three-dimensional finite element (3D FE) code MASA developed at the University of Stuttgart (Ožbolt 1998). Through a number of numerical studies it has been demonstrated that the code is able to realistically predict behaviour of concrete structures (Ožbolt *et al*. 2001, Ožbolt *et al*. 2002, Ožbolt and Reinhardt 2002, Ožbolt *et al*. 2000). In the analysis the concrete is simulated by the microplane model in which damage and cracking phenomena are modelled within the concept of smeared cracks. To assure mesh objective results relatively simple crack band approach is used (Bažant and Oh 1983).

It is important to note that for the realistic modelling of concrete the constitutive law plays the most important role. In the microplane model, the material response is calculated based on the monitoring of stresses and strains in different predefined directions. Integrating microplane stresses in a thermodynamically consistent way, from a known macroscopic strain tensor it is possible to calculate macroscopic stress tensor. The constitutive framework is similar to discrete type of the models (e.g. random particle model) with the difference that the model is formulated in the framework of continuum. The physical concept behind the microplane model was already discussed at the beginning of last century by Mohr (1900) and Taylor (1938). In the model, the material is characterized by uniaxial relations between stress and strain components on planes of various orientations. These planes may be imagined to represent damage planes or weak planes in the microstructure, such as those that exist at the contact between aggregate and the cement matrix. Unlike phenomenological models for concrete (e.g. plasticity or damage based models), which are

based on tensor invariants, in the microplane model the tensorial invariance restrictions need not be directly enforced. Superimposing, in a suitable manner, the responses from all the microplanes automatically satisfies them.

The used microplane model (Ožbolt *et al*. 2001) is based on the so-called relaxed kinematic constraint concept. It is a modification of the M2 microplane model proposed by Bažant and Prat (1988). Each microplane is defined by its unit normal vector components n_i (see Fig. 7). Microplane strains are assumed to be the projections of macroscopic strain tensor ε_{ij} (kinematic constraint). On the microplane are considered normal (σ_N, ε_N) and two shear stress-strain components (σ_K, σ_M, ε_K, ε_M).

To realistically model concrete, the normal microplane stress and strain components have to be decomposed into volumetric and deviatoric parts ($\sigma_N = \sigma_V + \sigma_D$, $\varepsilon_N = \varepsilon_V + \varepsilon_D$). Unlike most microplane formulations for concrete, which are based on the kinematic constrain approach, to prevent unrealistic model response for dominant tensile load and to prevent stress locking phenomena, in the present model kinematic constrain is relaxed by additional discontinuity function that is introduced at the macro level. Based on the micro-macro work conjugancy of volumetric-deviatoric split and using pre-defined microplane stress-strain constitutive laws, the macroscopic stress tensor is calculated as an integral over all possible, pre-defined, microplane orientations:

$$\sigma_{ij} = \sigma_V \delta_{ij} + \frac{3}{2\pi} \int_S \left[\sigma_D \left(n_i n_j - \frac{\delta_{ij}}{3} \right) + \frac{\sigma_K}{2} \left(k_i n_j + k_j n_i \right) + \frac{\sigma_M}{2} \left(m_i n_j + m_j n_i \right) \right] dS \qquad (1)$$

where S denotes the surface of the unit radius sphere and δ_{ij} denotes Kronecker delta and k_i and m_i are directions of shear microplane components. The integration is performed by numerical integration using 21 integration points (symmetric part of the sphere, see Fig. 7). For more detail see (Ožbolt *et al*. 2001).

3.2 Steel fibers

The constitutive law for fibers is defined by the uniaxial stress-strain relationship. The three-linear stress-strain law shown in Fig. 8 is used, which is defined by five parameters: initial Young's modulus E_0, hardening modulus E_h, yield stress f_y and tensile (compressive) strength f_s and limit strain ε_f. Once the strain reaches the limit value it is assumed that the stress immediately drops to zero. However, as will be shown later, in all here investigated cases the failure of steel was not relevant since the fibers were pulled-out before the limit strain was reached. The constitutive law is assumed to be the same for tension and compression.

3.3 Connection between fibers and concrete: discrete bond-slip relationship

The discrete bond model for the modelling of bond between concrete and deformed reinforcement bars is here used to simulate the connection between fibers and concrete (Ožbolt *et al*. 2002). In the finite element model the bond model simulates the connection between concrete 3D finite elements and the fibers that are represented by 1D truss finite elements. The connection perpendicular to the fiber orientation is assumed to be perfect and the connection in direction of

fiber axis is defined by discrete bond-slip law. The fiber slip s represents a relative displacement between "the same" concrete and the fiber node in direction of fiber axis. It is modelled using zero length nonlinear spring element. The equation used for the discrete bond model is divided into four parts (Ožbolt *et al*. 2002, see Fig. 9):

$$\tau(s) = \tau_0 \cdot \left(\frac{s}{s_0}\right) \cdot \left[\left(\frac{k_2}{k_1}\right) + \left(1 - \left(\frac{k_2}{k_1}\right)\right) \cdot \left(1 + \left(\frac{s}{s_0}\right)^R\right)^{-\frac{1}{R}}\right] \qquad \text{for} \quad s \le s_1$$

$$\tau(s) = \tau_m + \tau_f \qquad \text{for} \quad s_1 < s \le s_2$$

$$\tau(s) = \tau_m \cdot \left(\frac{s_3 - s}{s_3 - s_2}\right) + \tau_f \qquad \text{for} \quad s_2 < s \le s_3 \qquad (2)$$

$$\tau(s) = \tau_f \qquad \text{for} \quad s_3 < s$$

where the parameters for s (slip), τ (bond stress), k (stiffness) and R (radius of curvature of the ascending branch) are defined as shown in Fig. 9.

3.4 Generation of fiber finite elements

For the defined 3D space of the beam the fibers are generated randomly. For the given length of fibers (35 mm) the position of their centre of gravity and orientation are chosen as a random variables. The random generator fulfils two constrains: (1) the generation of fibers is terminated when in the advanced specified volume content of fibers is reached and (2) the crossing between fibers is not allowed, i.e. if two fibers are crossing one of them is removed. Once the fibers are generated they are discretized by four truss finite elements as a straight bars, i.e. the hooks are not modelled (see Fig. 10). Note that their mechanical effect is taken into account indirectly through the effective bond-slip relationship. Truss finite elements are used as a constraint for the generation of four node concrete solid finite elements. At the common points two nodes are introduced and connected with zero length nonlinear spring elements, which represent bond-slip constitutive law, as defined above.

In order to save computational time, in the 3-point bending finite element analysis of the beam, only central part of the beam (150x150x150 mm) is modelled as a three-phase material. The rest of the beam, which is out of the zone of interest, is modelled using standard 3D solid finite elements representing fiber reinforced concrete at macro scale. Furthermore, in the analysis simplified version of the bond-slip relationship from Fig. 9 is used in most cases with the assumption $R = \infty$ (see Fig. 10). The essential parameters for the calibration of the bond - slip relationship (τ-s) are: $k_1 = k_2 = k_{secant}$, $\tau_{max} = \tau_m + \tau_f$ and s_3. The contribution of the hooks is smeared out over the length of the fibers and it is represented by the mechanical bond (τ_m). The friction between deformed fiber and concrete is accounted for through τ_f. Both contributions are assumed to be the same in all five nodes of the fiber finite elements. This simplification is introduced in order to avoid modelling of complex processes related to the deformation of hooks when a fiber is pulled out from the concrete. In such modelling approach the fiber has to be discretized with several beam finite elements in

order to simulate pull-out from the concrete realistically. In the present simulations four finite elements are used.

4. Numerical analysis

4.1 Finite element model

The numerical analysis is carried out for notched beams with different fiber volume fractions (V_f=0%, 0.5%, 1.0% and 1.5%). For the finite element discretization of the beam with fiber content V_f=0.5 % and V_f=1 %, in total 1874 and 3784 fibers, respectively, are generated in the middle zone of the beam. For the fiber volume fraction of V_f=1.5 % the number of concrete 3D finite elements becomes extremely large and the analysis very demanding. Therefore, the finite element mesh for this case (V_f=1.5 %) is the same as for the case V_f=1.0 %, however, the cross-section area and diameter of the fibers are adopted accordingly, i.e. an increase of 1.5 times in the fiber cross section area and fiber circumference are accounted for. The models for plain concrete (V_f=0 %) are generated for concrete meshes that correspond to V_f=0.5 % and V_f=1.0 %. These two models are marked with V_f=0.0 % (0.5 %) and V_f=1.0 % (1.0 %), respectively. Note that the discretizations without bond elements and fibers need to be verified with respect to the mesh objectivity, i.e. two different meshes for plain concrete beams should result to the same response. The typical finite element discretizations for beams with 0.5 % and 1.0 % of volume fiber fractions together with random distribution of fibers are shown in Fig. 11.

4.2 Calibration of concrete parameters

The model parameters are obtained by fitting of the test results for plain concrete beams loaded in 3-point bending under displacement control. The experimentally obtained load-displacement curve for mean value is fitted by the numerical simulation. In Fig. 12 are shown stress-strain curves for uniaxial compression and tension, respectively. The curves are plotted for the crack band width (element size) $h = 5$ mm. The resulting macroscopic properties of concrete are: Young's modulus $E_c = 38652$ MPa, Poisson's ratio $v_c = 0.18$, uniaxial compressive strength $f_c = 75.0$ MPa, uniaxial tensile strength $f_t = 5.24$ MPa and fracture energy $G_F = 92$ J/m^2.

In Fig. 13 are plotted experimentally and numerically obtained curves for two different meshes. As can be seen the agreement between experimental and numerical results for plain concrete is reasonably good for both discretizations.

4.3 Effective bond - slip relationship of single fiber

The mechanical properties of steel fiber are given by the producer and are as follows: Young's modulus $E_s = 210$ GPa, Poisson's ratio $v_s = 0.33$, yield stress $f_y = 1.211$ GPa, strength $f_s = 1.345$ GPa, hardening modulus $E_h = 14.56$ GPa and limit strain $\varepsilon_s = 0.05$. The bond-slip relationship (τ-s) for single fiber is obtained from the single fiber pull-out test (see Fig. 3) with bond stress:

$$\tau = \frac{P}{(d_f \cdot \pi) \cdot l_e}$$

(3)

where P is the pull-out load, d_f is the fiber diameter (0.55 mm) and l_e is the embedment length (9 mm).

The model parameters of the effective bond-slip curve (see Fig. 9) for single fiber loaded in axial direction are obtained by fitting experimentally obtained bond-slip relationship (mean value, Fig. 3). Based on the fit, the discrete bond model parameters are obtained as: τ_m=10.17 MPa, τ_f=1.83 MPa, k_{secant}=17.129 MPa/mm, k_1=41.808 MPa/mm, k_2=2.707 MPa/mm, s_2^*=0.2 mm, s_3= 4.8 mm and R=3.039. The comparison between the experimental bond-slip curve and the constitutive law is shown in Fig. 14.

The influence of the bond-slip relationship on the response of the beam is first studied for the concrete mix with volume fiber fraction of 0.5%. The analysis is carried out using bond-slip constitutive law for pull-out of single fiber (case BS-P, see Table 1). The comparison with the experimental results (see Fig. 15) shows that the peak resistance is well estimated, however, the pre-peak stiffness is too low and the post peak response too brittle. There are two reasons for this, first, the bond-slip relationship for a single fiber does not account for the interaction between fibers (damage of concrete between fibers) and, second, in the critical section of the beam fibers are loaded (pulled out) in directions that do not coincide with the their axis, i.e. there is also dowel action, which leads to the increase of the stiffness of the effective bond-slip relationship. The analysis clearly shows that the initial stiffness of the bond-slip relationship significantly influences the response. Therefore, to more realistically estimate the effective bond-slip relationship, single fiber tests, where the inclination of fibers is varied, should be carried out. Moreover, additional numerical parametric study would be useful to investigate the effect in more detail.

To obtain better fit of the experimental results a parametric study is carried out. In the study the simplified version of the bond-slip relationship (see Fig. 10a) is used in which, compared to the single bond-slip relationship, stiffness k_1, k_2 and k_{secant} are increased and all equal to 1200 MPa/mm, keeping all other parameters the same (case BS-1, see Table 1). With these parameters for bond-slip relationship the analysis shows very good agreement with the experiments almost in the entire displacement range, up to 5 mm. To further improve the response for large displacements, in the next step slip parameter s_3 is slightly decreased, from 4.8 mm to 4.0 mm (case BS-2). The resulting curve obtained from the meso-scale model exhibit now nice agreement with the experimental curve, not only for the pre-peak response and resistance but also for the entire post-peak response in the range up to displacement of 5 mm. Finally, the effect of bond strength on the response of the beam is investigated by varying peak resistance (12.0 MPa, case BS-1) in the range of ±20 % (cases BS-3 and BS-4). From Fig. 15 can be seen that this leads to the positive and negative shift, respectively, of the post-peak response. Based on the comparison of the numerical and experimental data it can be concluded that the best fit for $V_f = 0.5$ % is obtained for the bond-slip relationship BS-2.

If one employs the bond-slip relationship obtained from the calibration of the model with $V_f = 0.5$ % for the beams with higher content of fibers then the resulting resistance is overestimated and the post-peak response is too ductile. This is illustrated in Fig. 16 which shows the comparison between the corresponding experimental data and numerical simulation using bond slip relationship for the case BS-2. The reason for this is obvious, namely, due to the higher content of fibers the interaction between fibers over the surrounding concrete leads to the reduction of the pull-out capacity of fibers. The concrete of the fracture process zone between fibers becomes more damaged and consequently the pull-out capacity of fibers is lower.

The evaluation of numerical results shows that the effective bond-slip relationship should be

adapted to the volume content of fibers. This is obtained through the parametric study, similar as carried out for the fiber volume content of 0.5 %. In the study the starting constitutive bond-slip relationship is the case BS-2 (see Table 1). The peak resistance τ_m and the limit slip s_3 are varied such that the analysis fit the mean load-displacement curve for the fiber volume content of 1.0 % and 1.5 %, respectively. The optimal parameters of the bond-slip constitutive law for all three volume contents are summarised in Table 2 and the corresponding bond-slip relationships are plotted in Fig. 17.

The resulting load-displacement curves for the beams with volume fraction of fibers varied from 0 % to 1.5 % are shown in Fig. 18. As can be seen for the entire range of the post peak response the agreement between numerical and experimental curves is very good. Note that for the case with 1% of fiber content the analysis was stopped at displacement of approximately 4 mm due to numerical difficulties. It can be seen that for relative low volume fraction of fibers after the peak resistance is reached the load-displacement curve exhibit a sudden drop and subsequent recovery. This is due to the relative low volume content of fibers but is also dependent on the beam size. In case of large beams this drop would probably be even more pronounced.

In all simulations the failure is due to the bending Mode-I failure type. For the lower content of fibers damage tends to be more localized around the final discrete crack whereas for the cases with higher content of fibers damage tends to be more distributed. Typical crack patters observed in the experiments and analyses for $V_f = 1.0$ % and 1.5 %, respectively, are shown in Fig. 19. It can be seen that concrete in the fracture process zone is more damaged if the content of fibers is higher (compare Figs. 19c and 19d). This explains the reason for decrease of effective bond resistance of fibers with increase of volume fractions of fibers.

In Table 3 are summarized the maximum and minimum stresses in fibers. It is evident that in no case the stress in the fibers reaches yield stress f_y=1210.5 MPa. Moreover, the maximum tensile stresses in fibers descreases with increase of volume fraction of fibers. In the contrary, the compressive stresses in fibers increases with increase of volume fraction of fibers. Obviously, failure is due to the pull-out of fibers and not to the failure of steel. This suggests that for the correct prediction of the failure of beams the pull-out constitutive law is relevant.

The importance of the bond-slip constitutive law is demonstrated in Fig. 20, which shows load-displacement response of the beam ($V_f = 0.5$ %) assuming three different bond-slip relationships: (1) bond-slip law the same as in the case BS-2 (see Table 1), (2) perfect bond (no slip) and no limit strain of steel and (3) perfect bond and limit strain failure of steel equal to 5 %. From Fig. 20 can be seen that perfect bond leads to high peak resistance and high ductility only if no failure of steel fibers takes place. With accounting for the limit on the strain in steel (5 %) peak load also increases, however, once the strength of steel fibers is reached there is relative brittle failure of the beam.

4.4 Proposed bond-slip relationship

Based on the results of the numerical study the correlation between the maximum shear stress $\tau_{max}=\tau_m+\tau_f$ [MPa] and the fiber volume fraction V_f [%] is proposed as:

$$\tau_{\max}(V_f) = \tau_{\max,s} \qquad\qquad 0 \leq V_f < 0.5$$
$$\tau_{\max}(V_f) = A + \frac{B}{V_f} \qquad\qquad 0.5 \leq V_f < 1.5 \tag{4}$$

where $\tau_{max,s}$ is the bond strength of a single fiber and A and B are constants obtained from the above discussed fitting procedure. For the fibers investigated in the present study $\tau_{max,s} = 12$ MPa, A = 4.05 [MPa] and B = 3.97 [MPa] with correlation coefficient equal 0.99.

The correlation between the slip s_3 [mm] at which τ_m becomes zero and the fiber volume fraction V_f [%] is proposed as follows:

$$s_3(V_f) = s_{3,max} \qquad\qquad 0 \leq V_f < 0.5$$
$$s_3(V_f) = C + \frac{D}{V_f} \qquad\qquad 0.5 \leq V_f < 1.5 \tag{5}$$

in which $s_{3,max}$ is the maximum value of s_3 (4.0 mm), which approximately corresponds to single pull-out constitutive law, C (1.0 mm) and D (1.5 mm) are a constants obtained from the fitting procedure with correlation coefficient 1.00. The relationships from (4) and (5) are plotted in Fig. 21. They can be used for the estimation of the parameters τ_{max} and s_3 for any fiber volume fraction value between 0.0 % and 1.5 %. Of course, these functions are valid only for the fiber type used in the present study. Moreover, they could also be dependent on the concrete type.

The above equations principally cover the the range of the volume content of fibers from 0.5% up to 1.5%, since for this range the study was carried out. However, for relatively low amount of fibers ($V_f < 0.5\%$) it is assumed that the distance between the fibers is such that the effective bond-slip resistance is not affected, i.e. the maximum bond resistance is reached for $V_f = 0.5\%$.

5. Conclusions

Based on the results of the study, the following conclusions can be drown out.

- The present numerical results show that meso scale approach based on the microplane model for concrete and discrete bond-slip relationship for steel fibers is able to realistically replicate experimental tests. As expected, with increase of the volume fraction of fibers the resistance and especially ductility increases.
- The effective bond-slip relationship is calibrated based on the fit of the experimental results for 3-point bending test data by the numerical results using bond-slip relation of a single fiber as the starting relationship.
- It is shown that the effective bond-slip relationship cannot be obtained only from a single fiber pull-out experiments, where the fibers were aligned with the loading direction. Single fiber tests, where the inclination of fibers is varied, can lead to a better representation of effective bond properties. From such a test only bond strength and maximum slip can be realistically evaluated. However, the initial stiffness is underestimated, with a consequence that the resulting pre-peak resistance is underestimated and the post-peak response is too brittle.
- With the increase of the volume content of fibers the bond strength and maximum slip decrease. The likely reason is the interaction among the fibers when they come too close to each other, i.e. the local damage of concrete around fibers leads to degradation of effective bond capability.

- The evaluation of the numerical results shows that for the investigated beams the failure is due to the failure of bond between concrete and fibers, i.e. fibers are pulled-out from the concrete. In all cases the yield stress in steel is not reached.
- All beams fail in mode-I bending failure type. With increase of the volume content of fibers local damage around discrete bending crack increases, which also leads to the increase of ductility.
- The proposed meso scale model is shown to be powerful numerical tool able to realistically predict behaviour of fiber reinforced concrete. In combination with experimental results it can be effectively employed in design of new steel fiber reinforced concretes and structural elements.

References

ACI Committee 544. (2001), "State-of-the Art Report on Fiber Reinforced Concrete", *ACI Manual of Concrete Practice*, ACI 544.1R-96.

Bažant, Z.P. and Oh, B.H. (1983), "Crack band theory for fracture of concrete", *RILEM*, **93**(16), 155-177.

Bažant, Z.P. and Prat, P.C. (1988), "Microplane model for brittle-plasic material-parts I and II", *Journal of Engineering Mechanics*, ASCE, **114**, 1672-1702.

Bolander, J.E., Choi, S. and Duddukuri, S.R. (2008), "Fracture of fiber-reinforced cement composites: Effects of fiber distribution", *International Journal of Fracture*, **154**, 73-86.

Bolander, J.E. and Saito, S. (1997), "Discrete modelling of short-fiber reinforcement in cementitious composites", *Advanced Cement Based Material*, **6**, 76-86.

Bolander, J.E. and Sukumar, N. (2005), "Irregular lattice model for quasistatic crack propagation", *Physical Review B*, **71**, 1-12.

EN 12390-3:2001 (2001), Testing hardened concrete - Part 3, Compressive strength of test specimens, Bruxelles.

EN 12390-6:2000 (2000), Testing hardened concrete - Part 6, Tensile splitting strength of test specimens, Bruxelles.

Caner, F.C., Bažant, Z.P. and Wendner, R. (2013), "Microplane model M7f for fiber reinforced concrete", *Engineering Fracture Mechanics*, **105**, 41-57.

Fischer, G., Stang, H. and Dick-Nielsen, L. (2007), "Initiation and development of cracking in ECC materials: experimental observations and modelling", *Fracture mechanics of concrete and concrete structures FRAMCOS6*, 1517-1522.

Han, T.-S., Feenstra, P.-H. and Billington, S.-L. (2003), "Simulation of highly ductile fiber-reinforced cement-based composite components under cyclic loading", *ACI Structural Journal*, **100**(6), 749-757.

Jun, P. and Mechtcherine, V. (2010), "Behaviour of strain-hardening cement-based composites (SHCC) under monotonic and cyclic tensile loading: Part 2 - Modelling", *Cement & Concrete Composites*, **32**, 810-818.

Kang, J., Kim, K., Lim, Y.M. and Bolander, J.E. (2014), "Modeling of fiber-reinforced cement composites: Discrete representation of fiber pullout", *International Journal of Solids and Structures*, **51**, 1970-1979.

Kunieda, M., Ogura, H., Ueda, N. and Nakamura, H. (2011), "Tensile fracture process of Strain Hardening Cementitious Composites by means of three-dimensional meso-scale analysis", *Cement & Concrete Composites*, **33**, 956-965.

Maalej, M. (2001), "Tensile properties of short fiber composites with fiber strength distribution", *Journal of Materials Science*, **36**, 2203-2212.

Mohr, O. (1900), "Welche Umstände bedingen die Elastizitätsgrenze und den Bruch eines Materiales?", *Zeitschrift des Vereins Deutscher Ingenieure*, **46**, 1524-1530, 1572-1577.

Ogura, H., Kunieda, M. and Nakamura, H. (2013), "Meso-Scale Analysis Considering Effect of Fiber Inclination in Fiber Reinforced Cementitious Composites", *RILEM Bookseries,* **8**, 261-272.

Ožbolt, J. (1998), "MASA – **MA**croscopic **S**pace **A**nalysis, Internal Report", Institut für Werkstoffe im Bauwesen, Universität Stuttgart.

Ožbolt, J., Meštrović, D., Li, Y.J. and Eligehausen, R. (2000), "Compression failure –beams made of different concrete types and sizes", *Journal of Structural Engeneering*, ASCE, **126**, 200-209.

Ožbolt, J., Li, Y.J. and Kožar, I. (2001), "Microplane Model for Concrete with Relaxed Kinematic Constraint", *International Journal of Solids and Structures*, **38**, 2683-2711.

Ožbolt, J., Lettow, S. and Kožar, I. (2002) "Discrete Bond Element for 3D Finite Element Analysis of Reinforced Concrete Structures". In Balázs-Bartos-Cairns-Borosnyói (eds), Proceedings of the 3rd International Symposium: *Bond in Concrete - from research to standards*, Budapest, University of Technology and Economics.

Ožbolt, J. and Reinhardt, H.W. (2002), "Numerical study of mixed mode fracture in concrete", *International Journal of Fracture*, **118**, 145-161.

Schauffert, E.A. and Cusatis, G. (2012), "Lattice Discrete Particle Model for Fiber-Reinforced Concrete. I: Theory", *Journal of Engineering Mechanics*, **138**, 826-833.

Schauffert, E.A., Cusatis, G., Pelessone, D., O'Daniel, J.L. and Baylot J.T. (2012), "Lattice Discrete Particle Model for Fiber-Reinforced Concrete. II: Tensile Fracture and Multiaxial Loading Behavior", *Journal of Engineering Mechanics*, **138**, 834-841.

Suwada, H. and Fukuyama, H. (2006), "Nonlinear finite element analysis on shear failure of structural elements using high performance fiber reinforced cement composite", *Journal of Advanced Concrete Technology*, **4**(1), 45-57.

Taylor, G.I. (1938), "Plastic strains in metals", *Journal of the Institute of Metals*, **62**, 307-324.

Vandewalle, L. (2002), "RILEM TC162-TDF Test and desig methods for steel fiber reinforced concrete: Bending test final Recommendation", *Materials and Structures*, **35**, 579-582.

Figures and Tables
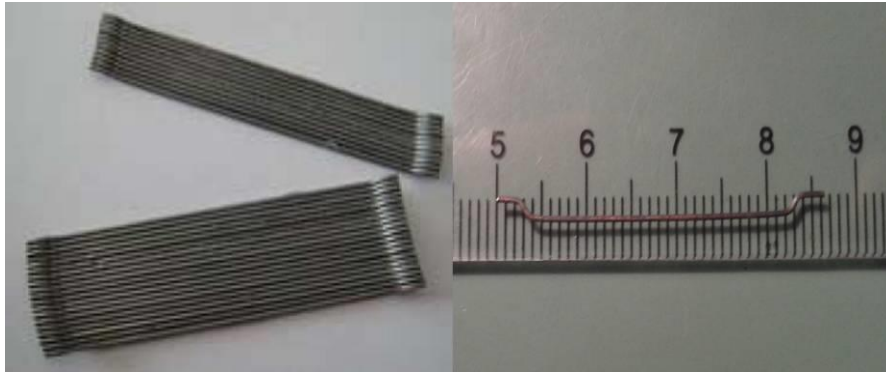
Fig. 1 Hook-ended steel fibers Dramix RC 65/35 BN
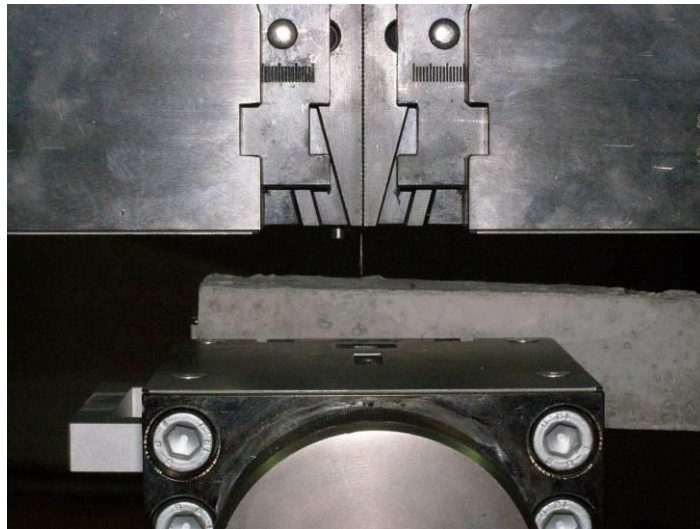
Fig. 2 Single fiber pull-out test
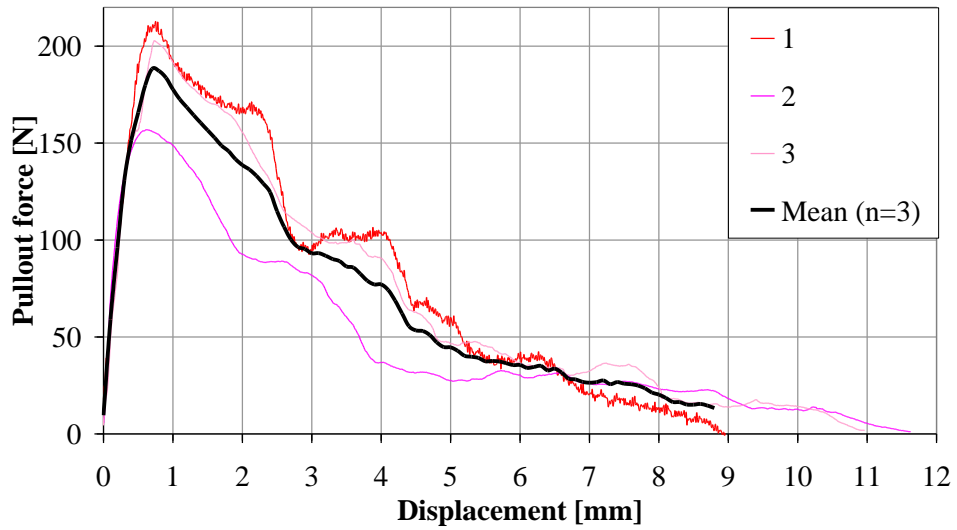
Fig. 3 Single fiber pull-out force vs. slip curves
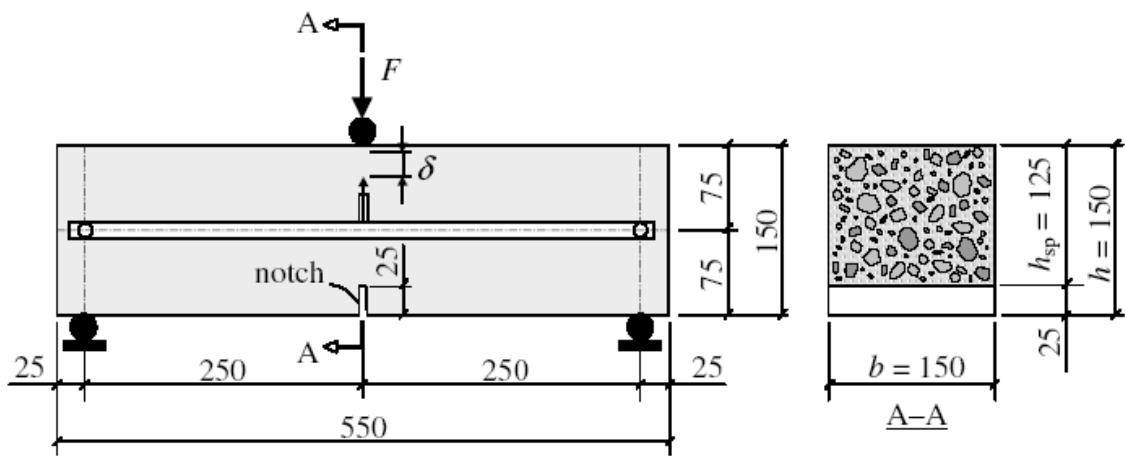
Fig. 4 Pre-notched beam geometry and 3-point bending test set-up (Vandewalle 2002)

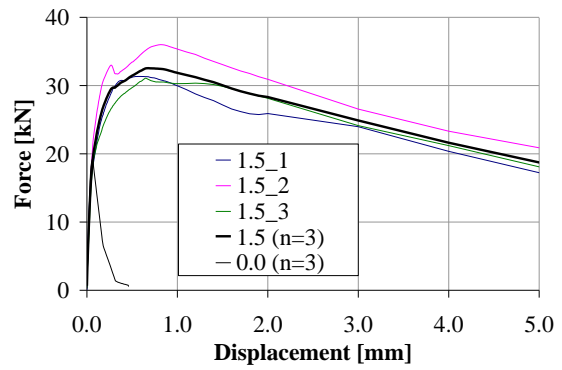Fig. 5 Displacement controlled flexural 3-point bending test set-up (V_f=1.5 %)
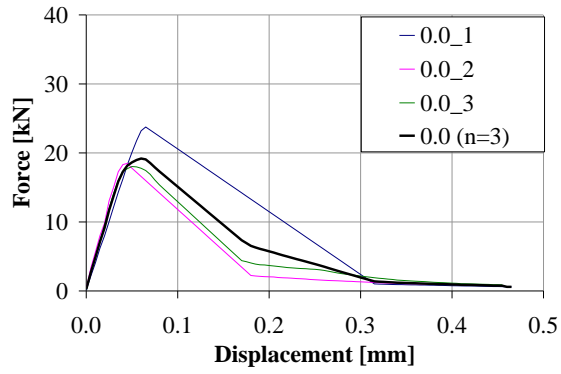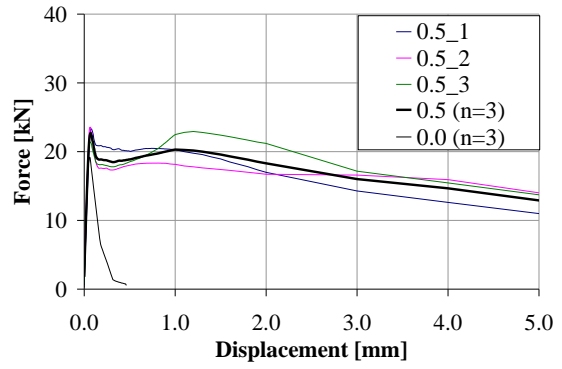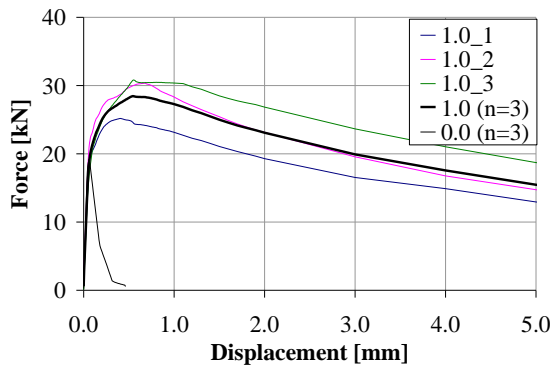
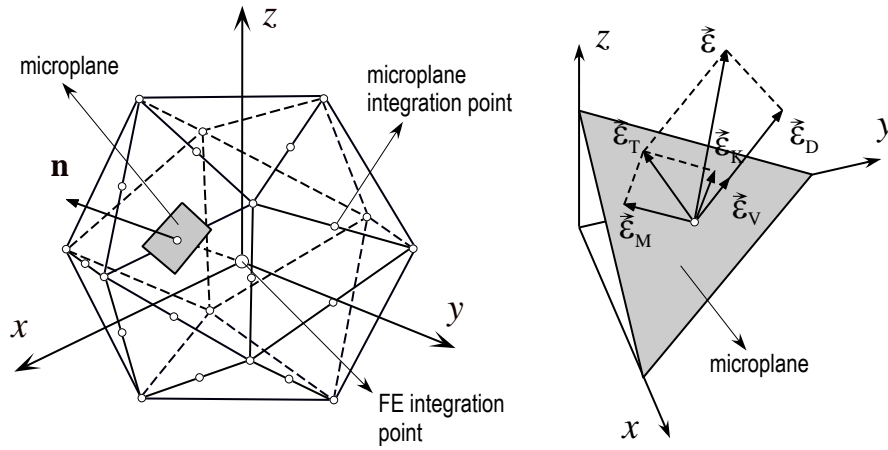Fig. 6 Experimentally measured load - displacement curves for beans with different fiber volume fractions

Fig. 7 Decomposition of the macroscopic strain vector into microplane strain components – normal (volumetric and deviatoric) and shear
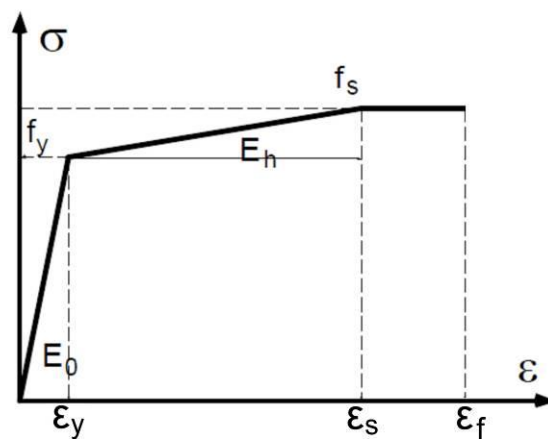
Fig. 8 Constitutive law of steel fiber
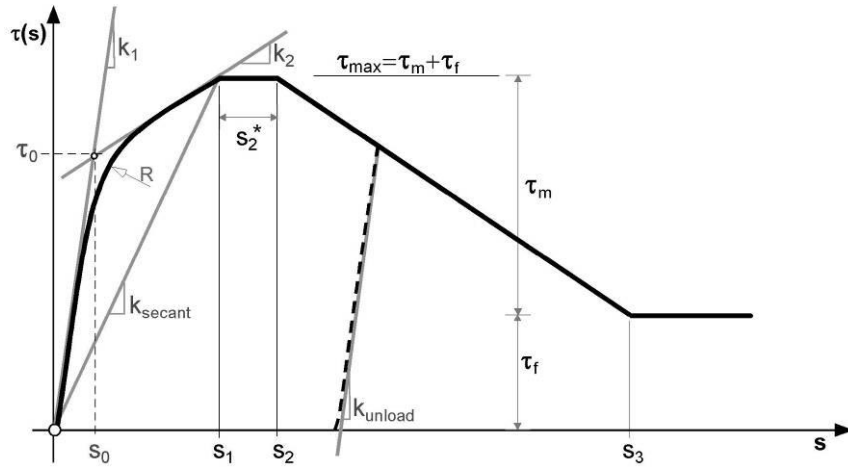
Fig. 9 Discrete bond-slip relationship
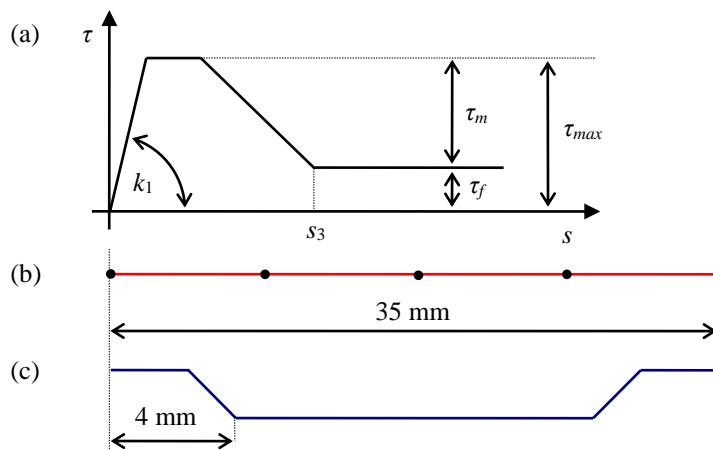
Fig. 10 Finite element idealization of fibers: (a) bond-slip relationship, (b) four truss finite elements and (c) actual fiber shape

(a)

(b)

(c)

(d)

(e)
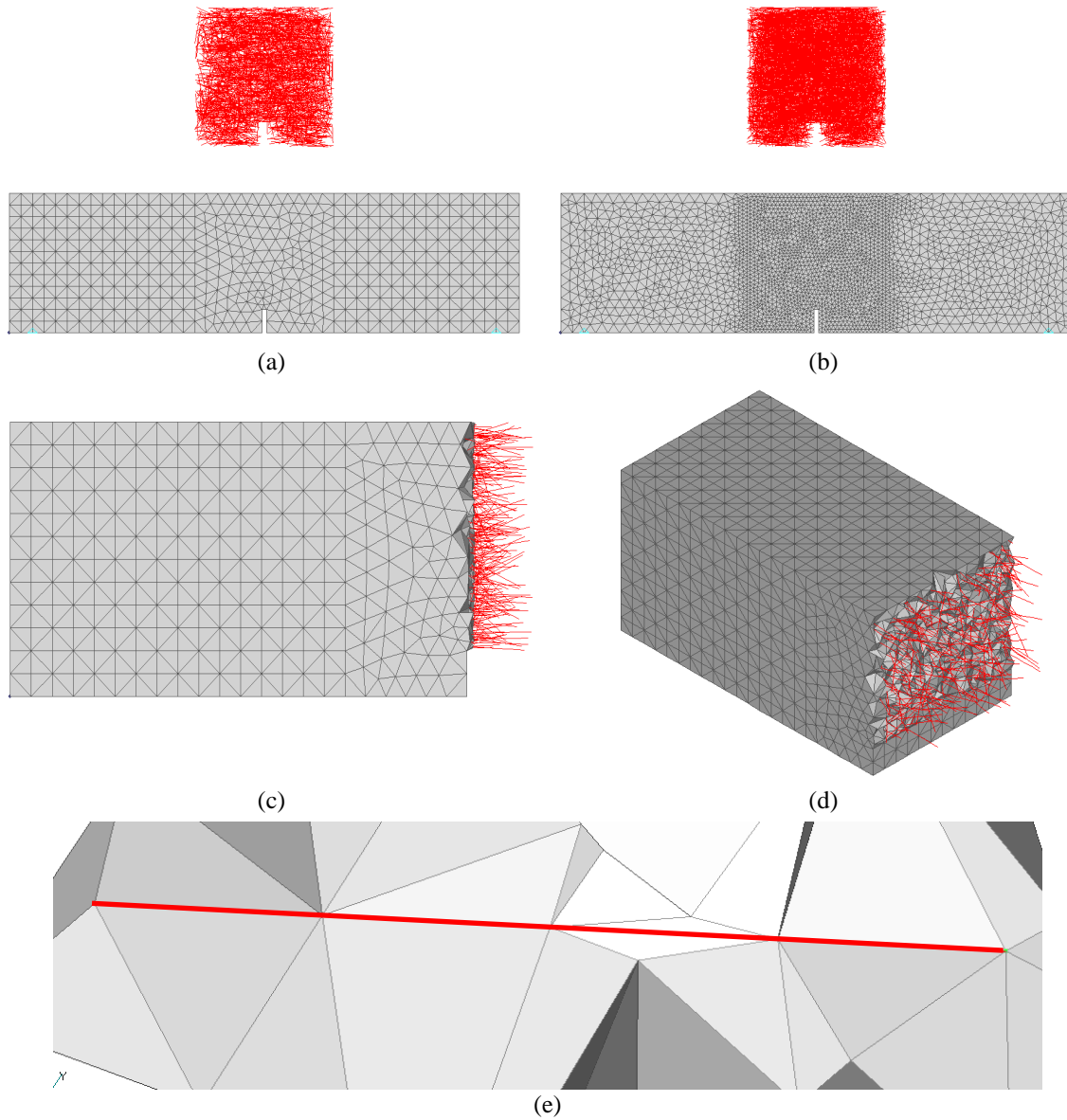
Fig. 11 Finite element discretization of concrete and fibers for fiber volume content of 0.5 % and 1.0 %: (a) V_f=0.5 %, entire beam view, (b) V_f=1.0 %, entire beam view, (c) V_f=0.5 %, left half of the beam (d) V_f=0.5 %, isometric view of the left half of the beam and (e) detail of fiber-concrete of connection

(a)   (b)
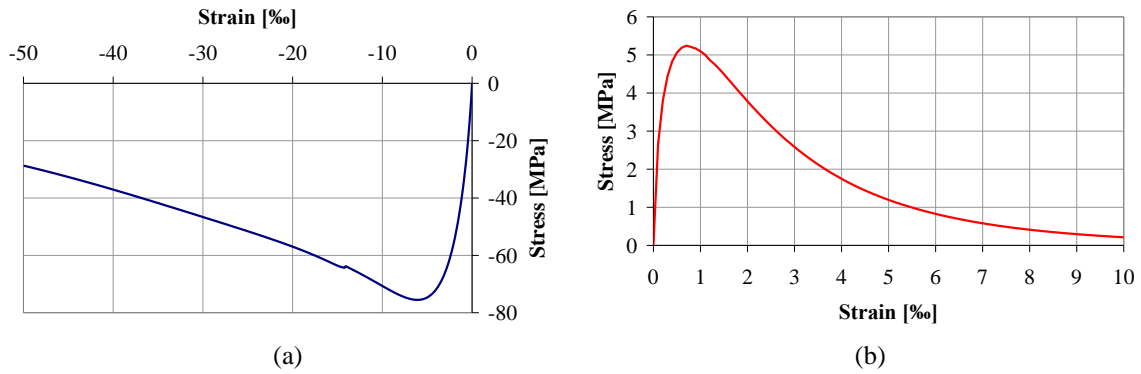
Fig. 12 Stress-strain curves for concrete: (a) uniaxial compression and (b) uniaxial tension
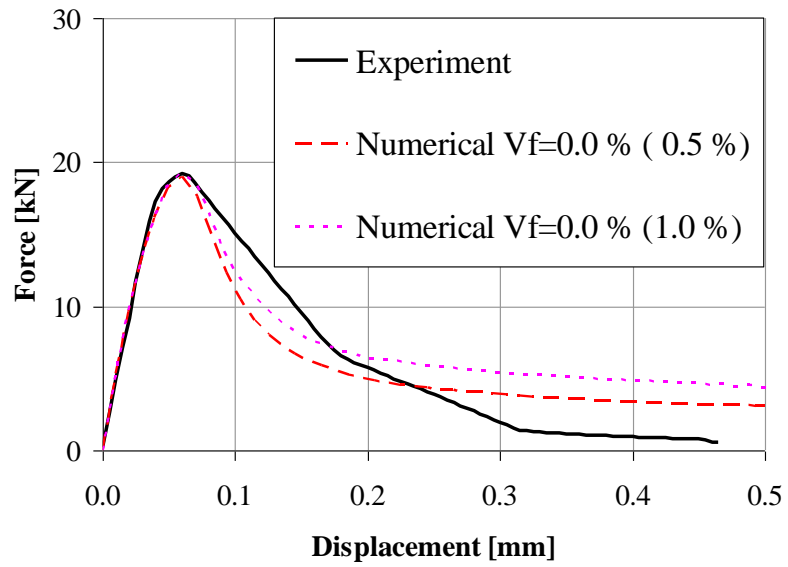
Fig. 13 Load-displacement curves for plain concrete beam, numerical and experimental results
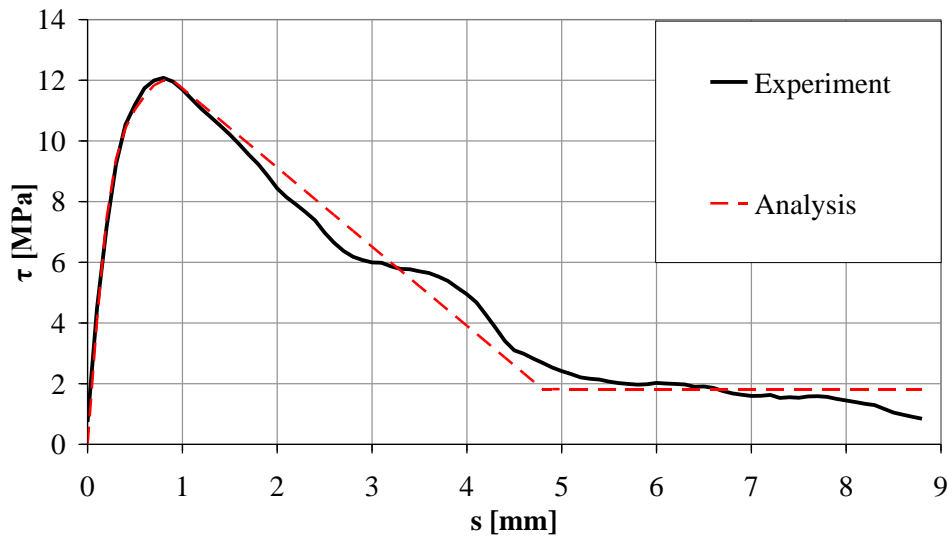
Fig. 14 Experimental single fiber bond - slip relationship (τ-s) and fit obtained from numerical analysis
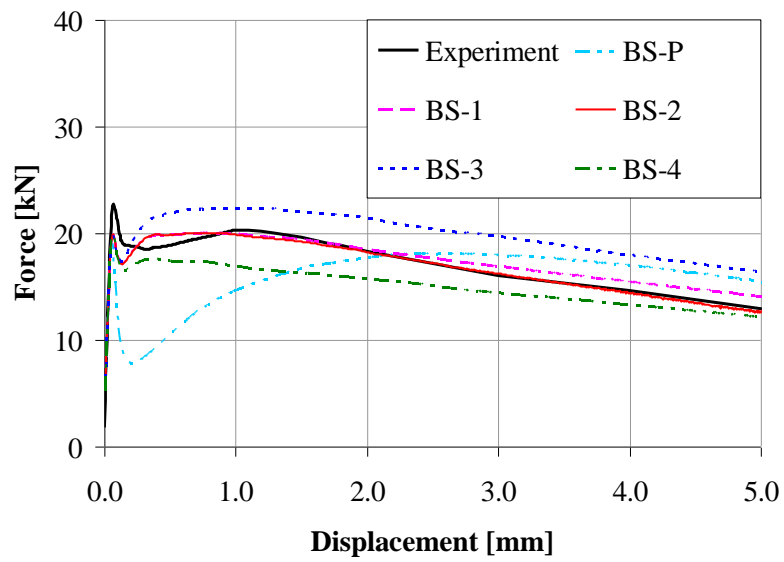
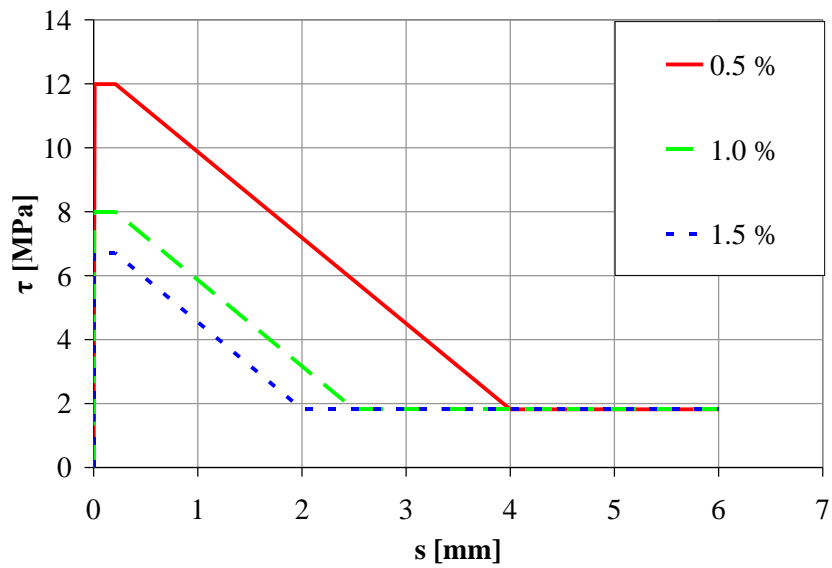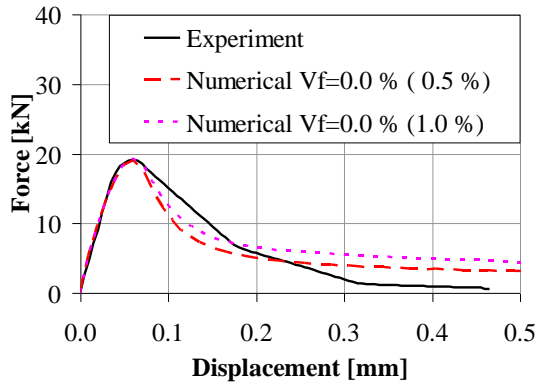Fig. 15 Comparison between experimentally and numerically obtained load – mid span displacement curves (V_f=0.5%) for different bond-slip relationships
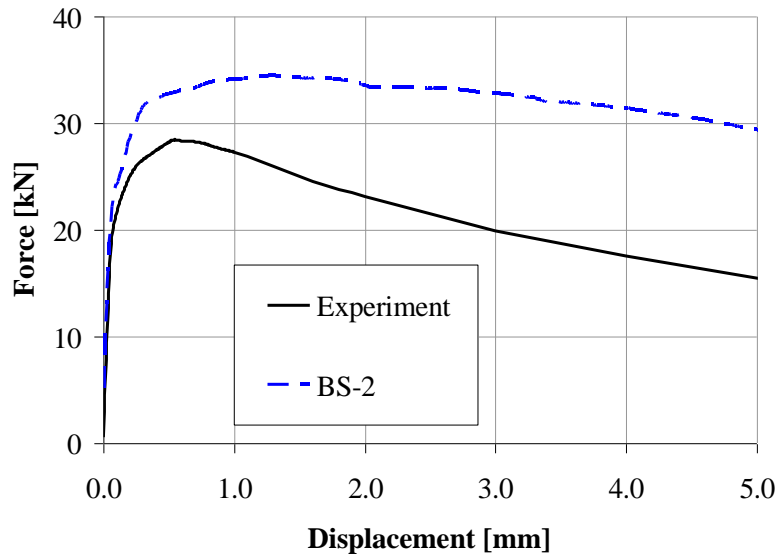
Fig. 16 Comparison between experimentally and numerically obtained load – mid span displacement curves
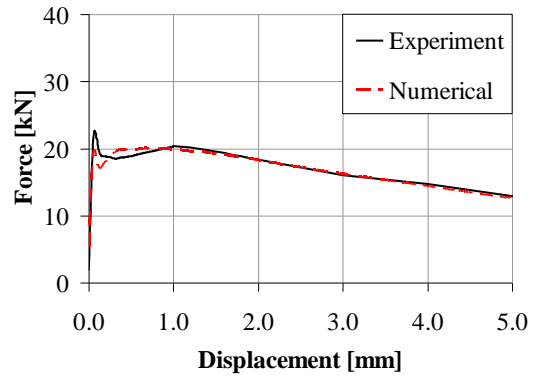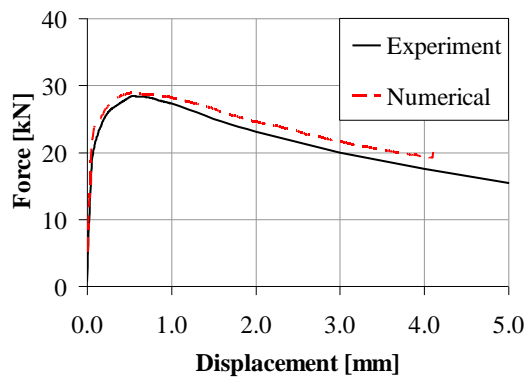(V_f=1.0%)

Fig. 17 Fiber bond - slip relationship (τ-s) for fiber reinforced concrete beams with different fiber volume
fractions

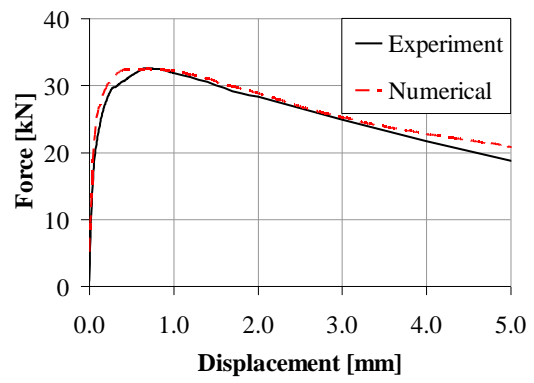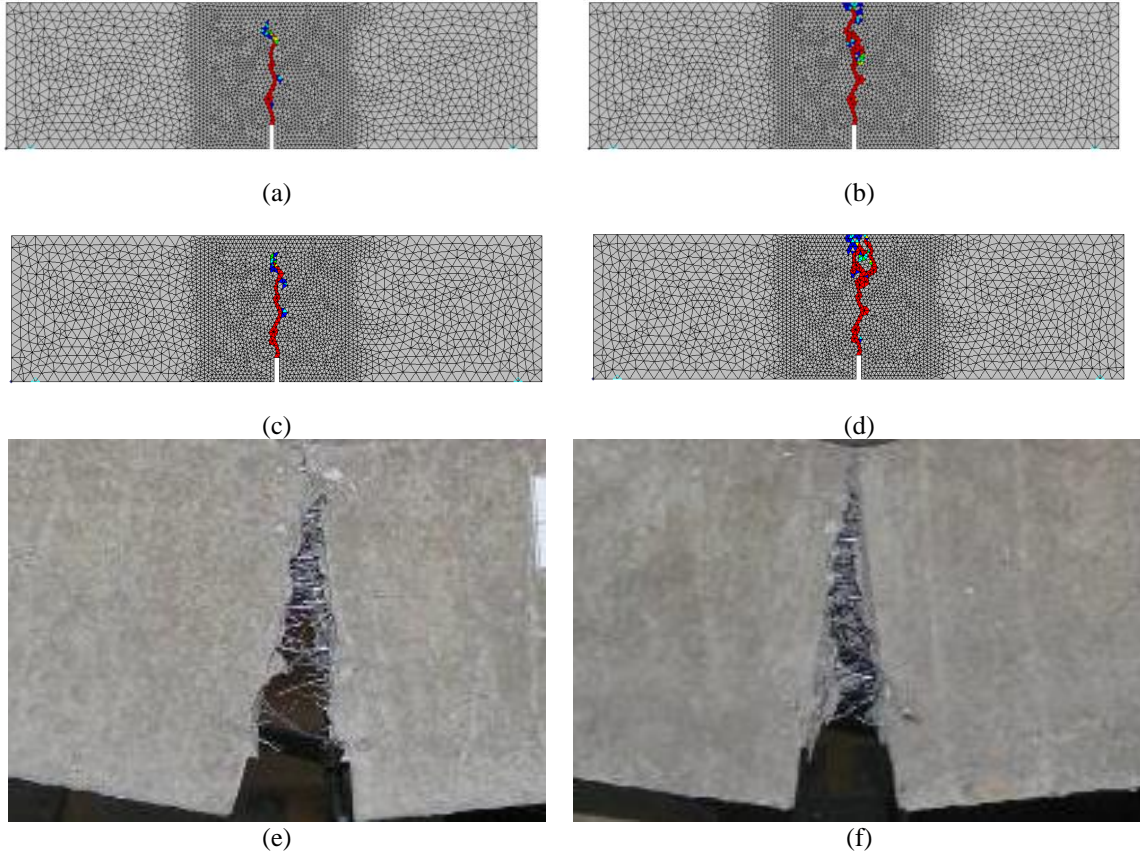Fig. 18 Comparison between experimentally and numerically obtained load – mid span deflection curves

Fig. 19 Cracks (maximum principal strain) at peak load: (a) V_f=1.0% and (b) V_f=1.5% and in the last increment: (c) V_f=1.0% and (d) V_f=1.5%; Experimental failure mode for: (e) V_f=1.0% and (f) V_f=1.5%
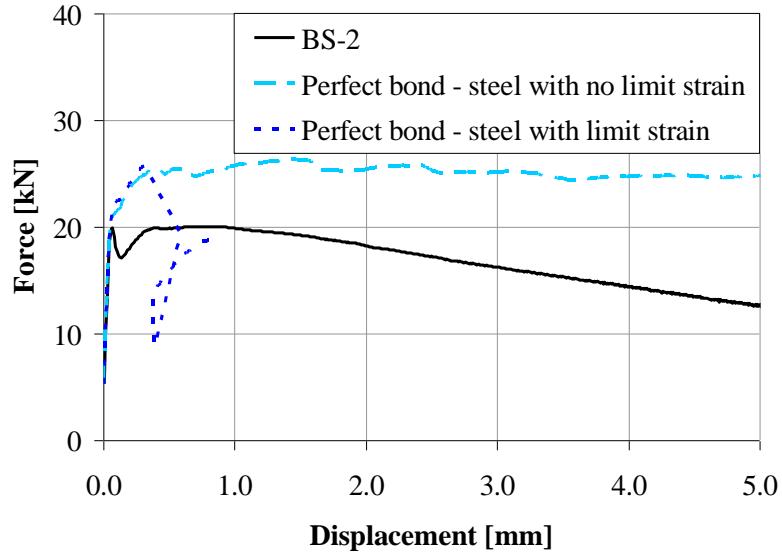
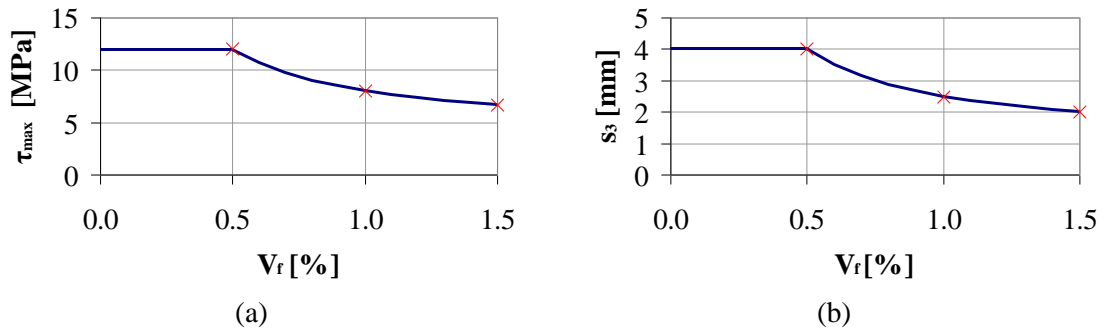Fig. 20 Load-displacement response of the beam ($V_f = 0.5\%$) assuming three different bond-slip relationships

(a)

(b)

Fig. 21 The correlation between (a) maximum bond strength (τ_{max}) and volume fraction of fibers (V_f) and (b) limit slip (s_3) and volume fraction of fibers (V_f)

Table 1 Discrete bond model parameters for $V_f = 0.5\%$

Case	Model parameters							
	τ_m [MPa]	τ_f [MPa]	k_{secant} [MPa/mm]	k_1 [MPa/mm]	k_2 [MPa/mm]	s_2^* [mm]	s_3 [mm]	R
BS-P	10.17	1.83	17.13	41.81	2.71	0.20	4.80	3.04
BS-1	10.17	1.83	1200	1200	1200	0.20	4.80	-
BS-2	10.17	1.83	1200	1200	1200	0.20	4.00	-
BS-3	12.55	1.83	1200	1200	1200	0.20	4.80	-
BS-4	7.76	1.83	1200	1200	1200	0.20	4.80	-

Table 2 Discrete bond model parameters for all models

Volume content of fibers	Model parameters					
	τ_m [MPa]	τ_f [MPa]	k_{secant} [MPa/mm]	k_1 [MPa/mm]	s_2^* [mm]	s_3 [mm]
0.5	10.17	1.83	1200	1200	0.20	4.00
1.0	6.17	1.83	1200	1200	0.20	2.50
1.5	4.89	1.83	1200	1200	0.20	2.00

Table 3 Maximum and minimum stresses in fibers

Model V_f [%]	maximum stress in fibers [MPa]	minimum stress in fibers [MPa]
0.5	1154	-359
1.0	771	-741
1.5	648	-632